Detection of Adsorption of Ru(II) and Os(II) Polypyridyl Complexes on Gold and Silver Nanoparticles by Single-Photon Counting Emission Measurements

Wilhelm R. Glomm,[†] Selina J. Moses,[†] Matthew K. Brennaman,[‡] John M. Papanikolas,[‡] and Stefan Franzen*,[†]

Department of Chemistry, North Carolina State University, Raleigh, North Carolina 27695, and Department of Chemistry, University of North Carolina at Chapel Hill, Chapel Hill, North Carolina 27599

Received: February 23, 2004; In Final Form: August 23, 2004

The present study describes a new application of ruthenium(II) tris(bipyridine) ($Ru(bpy)_3^{2+}$) and osmium(II) tris(bipyridine) ($Os(bpy)_3^{2+}$) as phosphorescent labels for the quantification of surface binding of molecules to gold and silver nanoparticles. The fraction of $Ru(bpy)_3^{2+}$ and $Os(bpy)_3^{2+}$ that is in solution can be distinguished from the surface-bound fraction by the relative lifetimes and integrated emission yields as determined by time-correlated single-photon counting (TCSPC) spectroscopy. Complementary steady-state measurements were carried out to confirm surface attachment of the phosphorescent label molecules. Although the emission of solutions of $Ru(bpy)_3^{2+}$ and $Os(bpy)_3^{2+}$ is quenched proportional to the concentration of 10 nm Au or 20 nm Ag nanoparticles, the quenching is static and not diffusional quenching observed in Stern−Volmer plots. The results demonstrate that time-resolved spectroscopy provides a rapid method for the measurement of surface binding of labeled molecules on metallic nanoparticles. While steady-state measurements require the preparation of a series of samples with varying quencher concentrations and a reference, the method described herein requires a single sample plus reference. The mechanism for phosphorescence quenching on Au and Ag nanoparticles is discussed in terms of energy and electron transfer theories.

Introduction

The direct observation of molecular properties on nanoparticle surfaces has wide application as a means of probing the electronic properties and the electrostatic environment of the colloid surface. Colloidal constructs consisting of molecular layers on the surface of metal and semiconductor colloids may serve as electrochemical probes as well as optical probes.[1,2] For example, the study of surface-enhanced phenomena with Raman, IR, and other nonlinear spectroscopies relies on knowledge of the molecular structure and a model for the geometric relationship between molecules and the surfaces of colloids or nanoparticles. Investigation of the electrostatic environment suggests that the stabilizer has a profound effect on the electrostatic field at the surface of a nanoparticle. The electrostatic effect is important since it relates to interparticle repulsions that stabilize colloidal suspensions. Moreover, the preparation of stable nanoparticle constructs that use DNA or proteins as recognition elements requires an understanding of the effect of electrostatics on the particle surface. The nature of the adsorption process of macromolecules and biomolecules has an effect on both optical and electronic properties of molecules on surfaces.

Steady-state emission studies of molecules on surfaces have indicated that quenching occurs when molecules are in the vicinity of a metal.[3−5] Electron and energy transfer between Ru(II) and Os(II) polypyridyl complexes linked to polymers has been widely studied,[6−8] making these molecules ideal probes of the surface of metal nanoparticles. Recently, Murray and coworkers reported steady-state emission quenching of $Ru(bpy)_3^{2+}$ on Au nanoparticles with radii smaller than required for the colloids to exhibit plasmon bands.[4] Herein, we study the quenching of emission of ruthenium(II) tris(bipyridine) ($Ru(bpy)_3^{2+}$) and osmium(II) tris(bipyridine) ($Os(bpy)_3^{2+}$) on Au and Ag surfaces. The emission quenching is observed both in steady state and using time-correlated single-photon counting (TCSPC) emission measurements. Compared to steady-state emission measurements, TCSPC has the advantage that one can distinguish a component that contributes only a few percent to the total emission signal using the lifetime of that component. Furthermore, steady-state quenching experiments require the preparation of a series of samples with difference quencher concentrations. This is not desirable for applications in biological samples where the colloidal stability of the nanoparticle/protein suspension requires saturation of the nanoparticle surface with protein adsorbate. Moreover, the static quenching observed for molecules attached to the surface of nanoparticles is not expected to follow diffusional Stern−Volmer behavior and a general method is needed to measure the interaction of molecules with surfaces. These studies demonstrate the general utility of time-resolved emission spectroscopy for the detection and quantification of labeled molecules on nanoparticle surfaces.

Experimental Section

A. Materials. Ten nanometer trisodium citrate stabilized gold colloids and 20 nm trisodium citrate stabilized silver colloids were purchased from Ted Pella, Inc. More stable preparations of gold nanoparticles were obtained by replacement of citrate by $HS(CH_2)_7COOH$ (mercaptooctanoic acid, MO). Concentration of the gold sol was determined by the absorption at $\omega_{\text{Fröhlich}} = 19\,200\ \text{cm}^{-1}$ (521 nm) for 10 nm Au. Ruthenium(II) tris(bipyridine) ($Ru(bpy)_3^{2+}$) was purchased from Alfa Aesar. Osmium(II) tris(bipyridine) ($Os(bpy)_3^{2+}$) was obtained as a gift from T. J. Meyer.

* To whom correspondence should be addressed.
[†] North Carolina State University.
[‡] University of North Carolina at Chapel Hill.

10.1021/jp049184k CCC: $30.25
Published on Web 12/21/2004

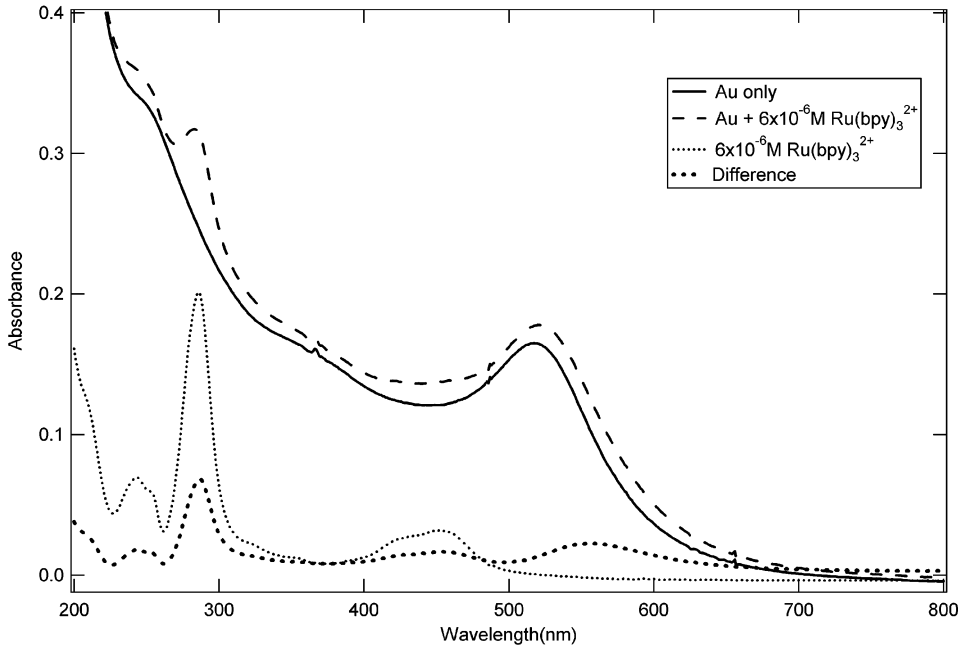

Figure 1. UV−vis absorption spectra of 6×10^{-6} M $Ru(bpy)_3^{2+}$ adsorbed onto 10 nm mercaptooctanoate (MO)-stabilized Au colloids (3.1×10^{-9} M), which corresponds to a ratio of $Ru(bpy)_3^{2+}/Au \approx 2000$. The mixture was allowed to equilibrate for ~1 h before spectra were taken. Monomer spectra of the Au colloids and the $Ru(bpy)_3^{2+}$ complex at equivalent concentrations are also included. The difference spectrum was obtained by subtracting the monomer spectrum of Au colloids from the spectrum of the mixture.

B. Steady-State Methods. All absorption measurements were made on a Hewlett-Packard 8453 Chemstation photodiode array spectrophotometer with attached Chemstation software using 0.5 cm cuvettes.

Steady-state emission spectra were recorded on a PTI Quantamaster luminescence spectrometer (MD-5020) or an ISS K2 phase fluorometer. Samples were sparged with argon prior to measurements.

C. Time-Resolved Emission Methods. The apparatus consists of a commercially available argon ion laser the continuous output of which is used to pump a mode-locked Ti:sapphire laser. The Ti:sapphire laser output is frequency-doubled to 423 nm using a BBO crystal to produce ~1 ps pulses with a pulse energy of ~0.26 nJ/pulse. This pulse train is pulse-picked, and the repetition rate is selected to be roughly 5 times the natural lifetime of the sample. Luminescence lifetime data was collected using the time-correlated single-photon counting technique described earlier.[6] Samples were sparged with argon for ~45 min prior to use.

Results

Steady-State Spectra. *System I: $Ru(bpy)_3^{2+}$ Adsorbed onto 10 nm MO-Stabilized Au Colloids.* Figure 1 shows the ground-state absorption spectrum of $Ru(bpy)_3^{2+}$ adsorbed onto 10 nm mercaptooctanoate (MO)-stabilized Au colloids. The spectrum shows an intense band centered at 521 nm, which corresponds to the Fröhlich frequency of 10 nm Au, as well as an additional band centered around 286 nm from the $Ru(bpy)_3^{2+}$ complex. From comparison with the monomer spectra, it is also possible to see the contribution from the metal-to-ligand charge transfer (MLCT) $Ru(bpy)_3^{2+}$ band centered at 450 nm. Upon adsorption, the shape and width of the Au plasmon band remained relatively unchanged, which confirms the presence of single colloids, and the peak of the gold plasmon band was shifted ~5 nm, indicating a slight change in the dielectric function of the Au surface that arises from the adsorption of $Ru(bpy)_3^{2+}$. The difference spectrum suggests that the $Ru(bpy)_3^{2+}$ bands are reduced in intensity.

The emission spectra for this system (see Supporting Information) clearly show the high-energy band around 590 nm from phosphorescence of $Ru(bpy)_3^{2+}$. The relative intensities of the emission of $Ru(bpy)_3^{2+}$ and $Ru(bpy)_3^{2+}$ on Au nanoparticles show that the presence of Au leads to quenching of the $Ru(bpy)_3^{2+}$ excited state. The emission data show that the contribution from the Au colloids themselves is negligible. The data presented in the Supporting Information show that there is clearly significant free (unbound) $Ru(bpy)_3^{2+}$ present and, as discussed below, most of the emission observed is likely to arise from the unbound fraction.

System II: $Ru(bpy)_3^{2+}$ Adsorbed onto 10 nm Citrate-Stabilized Au Colloids. The system depicted in Figure 2 shows essentially the same spectral features as the MO-stabilized system shown in Figure 1, taking into account that the $Ru(bpy)_3^{2+}$ concentration for the citrate-stabilized system is decreased by a factor of ~7 to adjust for the relative stabilizing properties of the passivating ligand (citrate versus MO). From the plasmon band of the Au colloids, the same conclusions can be drawn as for the MO-stabilized system; the $Ru(bpy)_3^{2+}$ is indeed adsorbed onto the colloids (although the shift is smaller), and the system is not aggregating. However, the difference spectrum shows that the citrate-stabilized system deviates from its MO-stabilized counterpart in that the bands of the $Ru(bpy)_3^{2+}$ are not bleached as a result of the adsorption. The MLCT band of $Ru(bpy)_3^{2+}$ is observed at a higher frequency than the plasmon frequency of Au. The emission spectra for this system (see Supporting Information) show the same trend as that observed for the MO-stabilized system. The relative intensities of $Ru(bpy)_3^{2+}$ and Ru−Au emission indicate that the presence of Au leads to extensive quenching of the $Ru(bpy)_3^{2+}$ excited state.

System III: $Ru(bpy)_3^{2+}$ Adsorbed onto 20 nm Citrate-Stabilized Ag Colloids. Figure 3 shows the ground-state absorption spectrum of $Ru(bpy)_3^{2+}$ adsorbed onto 20 nm citrate-stabilized Ag colloids. The spectrum shows an intense band centered at 400 nm, which corresponds to the Fröhlich frequency of 20 nm Ag, as well as an additional band centered around

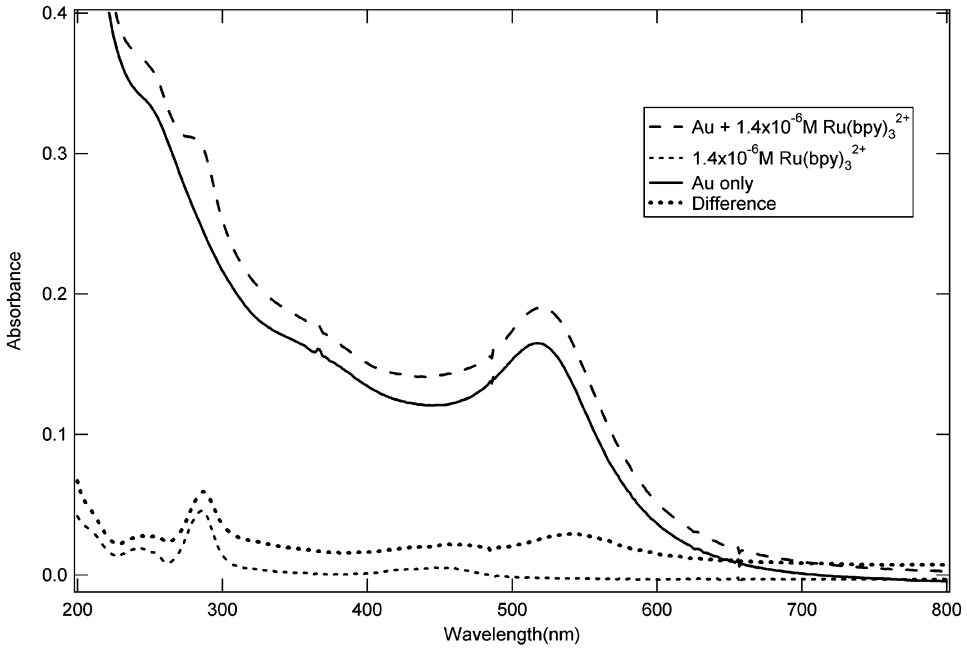

Figure 2. UV−vis absorption spectra of 1.4×10^{-6} M $Ru(bpy)_3^{2+}$ adsorbed onto 10 nm citrate-stabilized Au colloids (4.7×10^{-9} M), which corresponds to a ratio of $Ru(bpy)_3^{2+}$/Au ≈ 300. The mixture was allowed to equilibrate for ∼1 h before spectra were taken. Monomer spectra of the Au colloids and the $Ru(bpy)_3^{2+}$ complex at equivalent concentrations are also included. The difference spectrum was obtained by subtracting the monomer spectrum of Au colloids from the spectrum of the mixture.

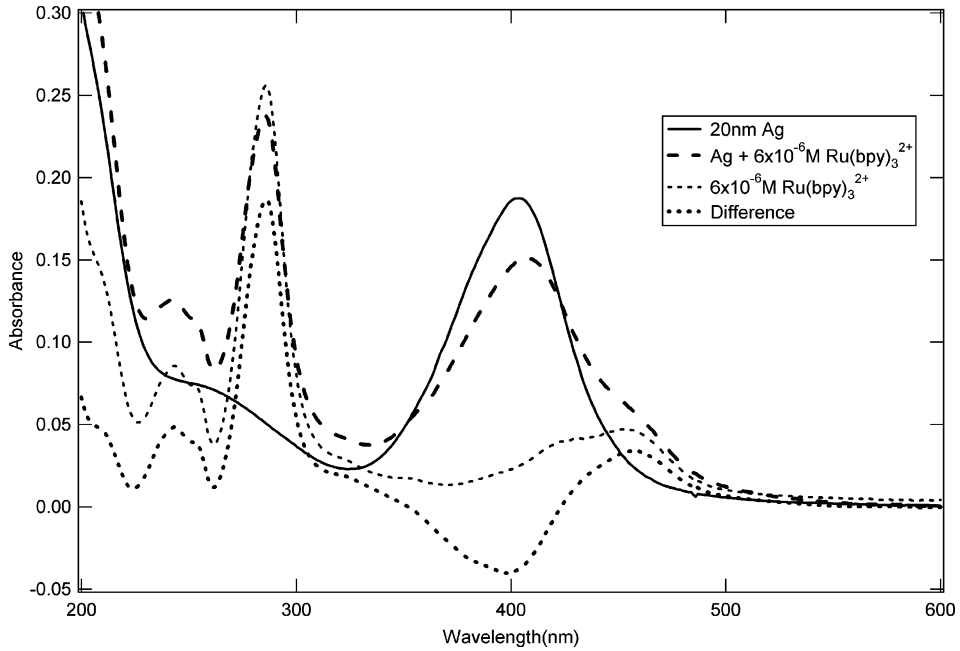

Figure 3. UV−vis absorption spectra of 6×10^{-6} M $Ru(bpy)_3^{2+}$ adsorbed onto 20 nm citrate-stabilized Ag colloids. The mixture was allowed to equilibrate for ∼2 h before spectra were taken. Monomer spectra of the Ag colloids and the $Ru(bpy)_3^{2+}$ complex at equivalent concentrations are also included. The difference spectrum was obtained by subtracting the monomer spectrum of Ag colloids from the spectrum of the mixture.

286 nm from the $Ru(bpy)_3^{2+}$ complex. From comparison with the monomer spectra, it is also possible to see the contribution from the MLCT band of $Ru(bpy)_3^{2+}$ centered at 450 nm. Upon adsorption, the shape and width of the Ag plasmon band remained relatively unchanged, confirming the presence of unaggregated colloids. The peak of the plasmon was shifted slightly (∼5 nm), indicating a slight change in the dielectric function of the Ag surface caused by the adsorption of $Ru(bpy)_3^{2+}$. As can be seen from the difference spectrum, altering the colloidal substrate from Au to Ag nanoparticles resulted in a substantial bleaching of the $Ru(bpy)_3^{2+}$ MLCT band at 450 nm, which is consistent with previous results for dye molecules on citrate-coated nanoparticles[9] (see below). The emission data (see Supporting Information) demonstrate that Ag-colloid and Au-colloid systems are comparable in their quenching and adsorption behavior; however, the colloidal stability of the Ag nanoparticles was much higher than that of Au nanoparticles.

System IV: $Os(bpy)_3^{2+}$ Adsorbed onto 20 nm Citrate-Stabilized Ag Colloids. Figure 4 shows the ground-state absorption spectrum of $Os(bpy)_3^{2+}$ adsorbed onto 20 nm citrate-stabilized Ag colloids. The spectrum shows an intense band centered at 400 nm, which corresponds to the Fröhlich frequency of 20 nm Ag, as well as bands from the $Os(bpy)_3^{2+}$ complex,

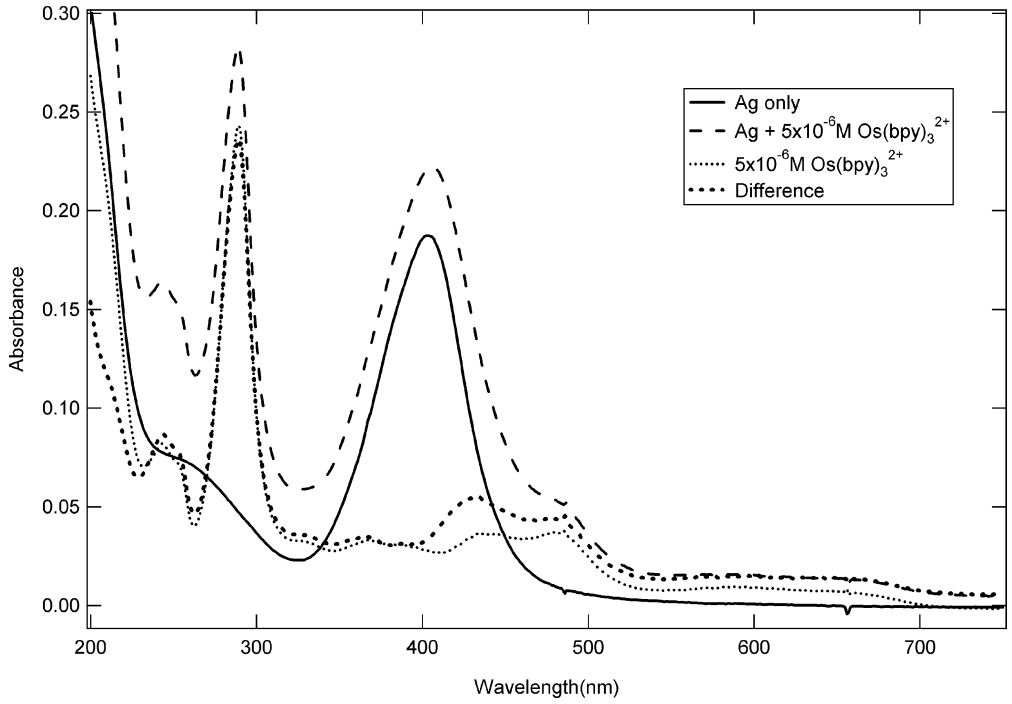

Figure 4. UV−vis absorption spectra of 5×10^{-6} M $Os(bpy)_3^{2+}$ adsorbed onto 20 nm citrate-stabilized Ag colloids. The mixture was allowed to equilibrate for ~1 h before spectra were taken. Monomer spectra of the Ag colloids and the $Os(bpy)_3^{2+}$ complex at equivalent concentrations are also included. The difference spectrum was obtained by subtracting the monomer spectrum of Ag colloids from the spectrum of the mixture.

TABLE 1: Lifetimes and Calculated Populations for Mixed Polypyridyl−Colloid Systems

adsorbate	substrate	lifetimes, τ (ns)	relative population	lifetime designation[a]
$Ru(bpy)_3^{2+}$		623.0	1.00	solution
$Ru(bpy)_3^{2+}$	10 nm Au[b]	0.8	0.60	surface
		4.5	0.12	surface
		605.3	0.31	solution
$Ru(bpy)_3^{2+}$	10 nm Au[c]	0.3	0.80	surface
		2.6	0.20	surface
$Ru(bpy)_3^{2+}$	20 nm Ag[c]	1.1	0.75	surface
		533.0	0.21	solution
$Os(bpy)_3^{2+}$		23.0	1.00	solution
$Os(bpy)_3^{2+}$	20 nm Ag[c]	0.4	0.54	surface
		22.0	0.42	solution

[a] Refers to the classification of an adsorbate and its relative population as either surface-confined or free in solution. [b] Mercapto-octanoate (MO)-stabilized Au colloids. [c] Trisodium citrate-stabilized colloids.

centered around 286 and 450 nm, and an additional, weaker band that extends out to ~700 nm. Upon adsorption, the shape and width of the Ag plasmon band remained relatively unchanged, which confirms the presence of unaggregated colloids, and the peak was shifted slightly, indicating a slight change in the dielectric function of the Ag surface that arises from the adsorption of $Os(bpy)_3^{2+}$. Interestingly, the emission data (see Supporting Information) suggest that the presence of Ag colloids quenches the intensity of the Os band centered around 720 nm much less than for the corresponding Ru system.

Time-Resolved Data. Time-resolved data were obtained for both the adsorbate systems and the colloidal substrate−adsorbate constructs. Table 1 summarizes the essential characteristics of each system, including the measured lifetimes. For all general functions used to fit the time-resolved data, see Supporting Information.

System I: Ru(bpy)$_3^{2+}$ Adsorbed onto 10 nm MO-Stabilized Au Colloids. Figure 5 shows the time-resolved data for 6 μM $Ru(bpy)_3^{2+}$ in aqueous solution. As expected, $Ru(bpy)_3^{2+}$ decays with single-exponential kinetics and a lifetime of 623 ns (trace A). Time-resolved emission data for the colloidal substrate−adsorbate constructs shown in Figure 5 demonstrate a clear deviation from this single-exponential behavior. System I, shown as trace B in Figure 5, has a biexponential decay. The biphasic fitting function was a five parameter function ($A_1 \exp\{-t/\tau_1\} + A_2 \exp\{-t/\tau_2\} + B$). The fit parameters were $A_1 = 0.68$ with

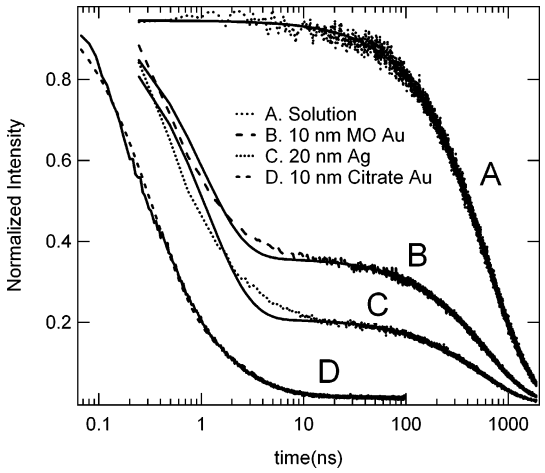

Figure 5. Time-resolved normalized emission from $Ru(bpy)_3^{2+}$ in solution and adsorbed onto various colloids. The colloids include 10 nm mercaptooctanoate (MO)-stabilized Au colloids (3.1×10^{-9} M), 20 nm citrate-stabilized Ag colloids, and 10 nm citrate-stabilized Au colloids (4.7×10^{-9} M). Given a solution concentration of 6×10^{-6} M $Ru(bpy)_3^{2+}$/Au for the MO-stabilized colloids, the ratio of $Ru(bpy)_3^{2+}$/Au is ~2000. Lower concentrations had to be used for the citrate-stabilized colloids to avoid aggregation. Given a solution concentration of 1.4×10^{-6} M $Ru(bpy)_3^{2+}$ in solution the ratio of $Ru(bpy)_3^{2+}$/Au was ~300. The excitation wavelength was 423 nm, and emission was detected at 640 nm. The experimental fits shown in the figure all used a biexponential function. Experimental data are shown as a dashed or dotted line, and the fit is shown as a solid line.

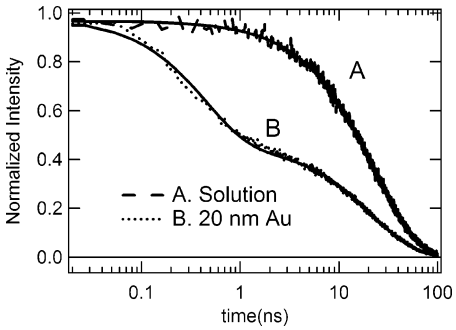

Figure 6. Time-resolved normalized emission data, detected at 780 nm, of 5×10^{-6} M $Os(bpy)_3^{2+}$ in aqueous solution and on 20 nm citrate-stabilized Ag colloids. The excitation wavelength was 423 nm. The experimental data for $Os(bpy)_3^{2+}$ in aqueous solution were fit to a single-exponential function, and the data for the mixed $Os(bpy)_3^{2+}$ colloid system were fit to a biexponential function. Experimental data are shown as a dashed line, and the fit is shown as a solid line.

$\tau_1 = 1.2$ ns and $A_2 = 0.31$ with $\tau_2 = 598$ ns and B = 0.01 (correlation coefficient of ~0.75). To improve the fit, a triexponential, seven parameter function ($A_1 \exp\{-t/\tau_1\} + A_2 \exp\{-t/\tau_2\} + A_3 \exp\{-t/\tau_3\} + B$) was used (see Table 1) resulting in a significant increase in the correlation coefficient from ~0.75 to ~0.93, thus suggesting that the emission at 640 nm in system I is comprised of three components.

System II: $Ru(bpy)_3^{2+}$ Adsorbed onto 10 nm Citrate-Stabilized Au Colloids. The adsorption of $Ru(bpy)_3^{2+}$ to 10 nm Au colloids with a trisodium citrate passivating layer required a concentration lower by a factor of roughly $^1/_7$ than that for system I. If the concentration is increased beyond that value, flocculation occurs. The data depicted in Figure 5 show a marked decrease in the phosphorescence lifetime for $Ru(bpy)_3^{2+}$ adsorbed onto the citrate-coated colloid. The data were fit to single-exponential, biexponential, and triexponential functions. A clear deviation from single-exponential decay was evident, but there was no significant improvement (<0.01) of the correlation coefficient upon adding a third exponential. The fit parameters for a biexponential model were $A_1 = 0.8$ with $\tau_1 = 0.32$ ns and $A_2 = 0.2$ with $\tau_2 = 2.6$ ns. As can be seen, none of these observed lifetimes were characteristic of unassociated $Ru(bpy)_3^{2+}$ ($\tau_{obs} = 623$ ns). These results indicate that essentially all of the $Ru(bpy)_3^{2+}$ is adsorbed onto, or at least associated with, the nanoparticle.

System III: $Ru(bpy)_3^{2+}$ Adsorbed onto 20 nm Citrate-Stabilized Ag Colloids. We collected spectral data for a transient of 5 μM $Ru(bpy)_3^{2+}$ adsorbed to 20 nm Ag colloids, as shown in Figure 5, to investigate the effect of changing the nature of the metallic substrate and to verify the assumption that the adsorbate concentration does not affect the number of species contributing to the emission. The data depicted in Figure 5 were treated in a fashion similar to that used for the previous data, resulting in a best fit for a biexponential decay, indicating one surface-confined species and one unattached species. The fit parameters were $A_1 = 0.75$ with $\tau_1 = 1.1$ ns and $A_2 = 0.21$, with $\tau_2 = 533$ ns. Addition of a third exponential resulted in little or no improvement of the correlation coefficient.

System IV: $Os(bpy)_3^{2+}$ Adsorbed onto 20 nm Citrate-Stabilized Ag Colloids. Figure 6 shows time-resolved data for 5 μM $Os(bpy)_3^{2+}$ in aqueous solution. Free $Os(bpy)_3^{2+}$ in solution decays with single-exponential kinetics with a lifetime of 23 ns. The mixed system was fit to a multiexponential decay and was best fit to a biexponential function. The fit parameters were $A_1 = 0.54$ with $\tau_1 = 0.40$ ns and $A_2 = 0.42$ with $\tau_2 = 22$ ns.

Discussion

The phosphorescence quenching observed in the time-resolved kinetic studies of $Ru(bpy)_3^{2+}$ is consistent with quenching observed in aromatic dye molecule adsorbates on Au and Ag nanoparticles.[3,9−11] In the present study, both Au colloids and Ag colloids were used to provide a comparison of different plasmon resonance frequencies. The plasmon bands of Ag and Au colloids are observed at higher and slightly lower energy than the MLCT band of $Ru(bpy)_3^{2+}$, respectively. The MLCT band of $Os(bpy)_3^{2+}$ is significantly lower in energy than the plasmon band of either Ag or Au colloids. If the molecular transition energy is lower than that of the plasmon resonance frequency of the metal colloid, the surface selection rules are consistent with absorption by any component of the transition moment perpendicular to the surface of the particle.[12] Since $Ru(bpy)_3^{2+}$ and $Os(bpy)_3^{2+}$ are nonplanar molecules, there must be components of the transition moment of the MLCT bands parallel and perpendicular to the surface so that some bleaching should be observed in the absorption spectrum. If the excitation were isotropic (i.e., no symmetry breaking), then one would expect that the intensity would be reduced by more than $^1/_2$. However, the electrostatic environment of the nanoparticle may lead to symmetry breaking that results in an oriented MLCT transition that favors excited-state charge-transfer to one bipyridine over the others.[13] There is some reduction in intensity for $Ru(bpy)_3^{2+}$ adducts on Au and Ag, but not for $Os(bpy)_3^{2+}$ adducts on Ag. The latter observation suggests that there is some symmetry breaking of the MLCT state in $Os(bpy)_3^{2+}$ on Ag nanoparticles.

The fact that there is substantial absorbance for surface-adsorbed $Ru(bpy)_3^{2+}$ suggests that a probe of the emission lifetime of the surface-bound fraction will provide a quantitative means to estimate the surface-bound fraction. For an idealized adsorption process between the adsorbate and the colloidal substrate, where the solute and adsorbate are in equilibrium and where adsorption does not progress beyond monolayer coverage, adsorbate emission would be expected to follow a single-exponential decay with a shorter lifetime than that of the solute (e.g., $Ru(bpy)_3^{2+}$ free in solution). In other words, a single-exponential decay would indicate that all of the $Ru(bpy)_3^{2+}$ is bound to the colloidal surface. A realistic model is comprised of a biexponential decay: a highly populated fast component representing the fraction of surface-bound $Ru(bpy)_3^{2+}$ and a less populated, slower component representing the fraction of $Ru(bpy)_3^{2+}$ still in solution. Such a model is consistent with static quenching because the luminescent molecule is immobilized on the surface of the metal colloid. The rate constant for quenching obtained from time-resolved measurements is significantly more rapid than that estimated from diffusional quenching (Stern−Volmer) model as indicated in the Supporting Information. The analysis of the surface-bound fraction by steady-state measurements proceeds based on the integrated emission yield of surface-bound species. We can compare the time-resolved and steady-state approaches for the normalized biexponential case. In a biexponential model, one molecular species (component 1) is free in solution and a second (component 2) is adsorbed to the nanoparticle.

$$I(t) = \phi_1 e^{-k_1 t} + \phi_2 e^{-k_2 t} \qquad \text{time-resolved} \qquad (1)$$

$$I = \phi_1 \int_0^\infty e^{-k_1 t}\, dt + \phi_2 \int_0^\infty e^{-k_2 t}\, dt = \frac{\phi_1}{k_1} + \frac{\phi_2}{k_2}$$

steady-state (2)

For normalized emission spectra $\phi_1 + \phi_2 = 1$, so the measured amplitudes in the time-resolved experiment correspond to the fraction of each species. Thus, it can be seen that the fractional population on the nanoparticle is obtained directly from a biexponential fit to the TCSPC data, while a steady-state measurement contains three unique parameters that must be separated.

The comparison of different passivating layers provides a means to examine the effects of surface adsorption in competition with different chemical groups. For example, citrate appears to be easily displaced from Au and Ag colloids compared to other passivating layers such as phosphines and alkane-thiols. The initial passivating layer, trisodium citrate, is displaced by the negatively charged alkane-thiols such as mercaptooctanoate, MO, through chemisorption of the thiol. In such an exchange process, it is possible that the new passivating layer has imperfections or that the fractional surface coverage of an adlayer such as MO is less than unity. Thus, surface adsorption of molecules can involve interaction with passivating layer or directly with the metal surface by displacement or at defect sites in the surface adlayer. Considering this, the triexponential function may provide a good and realistic fit and can physically be interpreted as the three components: (1) free $Ru(bpy)_3^{2+}$ (slowest component), (2) $Ru(bpy)_3^{2+}$ electrostatically adsorbed to the passivating layer on the colloidal surface, and (3) $Ru(bpy)_3^{2+}$ that displaces the passivating layer at the Au surface (fastest component).

The phosphorescence quantum yield is given by

$$\Phi_{\text{phosphorescence}} = \frac{k_{\text{phosphorescence}}}{k_q + k_{\text{ISC}} + k_{\text{phosphorescence}}} \qquad (3)$$

Equation 3 indicates that there is an intrinsic emission yield $\Phi_{\text{phosphorescence}} = k_{\text{phosphorescence}}/(k_{\text{ISC}} + k_{\text{phosphorescence}})$, where k_{ISC} is the intersystem crossing rate from the MLCT state back to the ground state. The observed phosphorescence yield for $Ru(bpy)_3^{2+}$ in deoxygenated solution is 0.042 ± 0.002 (at 25 °C).[14] Given that the observed phosphorescence rate constant in solution is $k_{\text{obs}} = k_{\text{ISC}} + k_{\text{phosphorescence}} = 1.61 \times 10^6$ s^{-1}, we have that the intrinsic phosphorescence rate constant is $k_{\text{phosphorescence}} = \Phi_{\text{phosphorescence}} k_{\text{obs}} = 6.72 \times 10^4$ s^{-1}. The quenching rate constant is significantly greater than the intersystem crossing rate constant.

The quenching process could arise from energy transfer, electron transfer, or an enhanced intersystem crossing rate constant. All of these quenching processes can be considered within the approximations of first-order time-dependent quantum mechanics. For energy transfer or electron transfer, the rate constant is

$$k_{\text{ET}} = \frac{\hbar^2}{2\pi} |V^2| \text{FC} \qquad (4)$$

where V is the electronic coupling and FC is the Franck−Condon factor. V is an electronic factor that can be expressed in terms of the electronic wave functions.

$$V = \langle \Psi_{\text{MLCT}} | H | \Psi_{\text{Ru}^{3+}\text{Au}^{-}} \rangle \qquad (5)$$

where Ψ represents the electronic wave function. The subscripts indicate that photoexcited state and one of the possible charge-separated states, respectively. The FC factor is given by

$$\text{FC} = \sum_{\nu,\nu'=0}^{\infty} \langle \chi_\nu^{\text{MLCT}} | \chi_{\nu'}^{\text{Ru}^{3+}\text{Au}^{-}} \rangle^2 \rho \qquad (6)$$

where χ_ν and $\chi_{\nu'}$ are the nuclear wave functions for the reactant and product states, respectively. The term ρ represents the density of states. The same formalism applies to ISC; however, in that case the Hamiltonian corresponds to the spin−orbit term. We regard an enhanced k_{ISC} rate constant as the least plausible mechanism.[15] Although Au may provide some perturbation to the spin−orbit term the central ruthenium in the $Ru(bpy)_3^{2+}$ adduct is likely to dominate. The density of phonon states near a metal is not the same as that in solution, but there is no evidence to support a large increase in the density of relevant phonon states.

It is often thought that energy transfer is responsible for quenching of luminescence due to dipolar transitions of a metal plasmon.[4,15−22] For a dipole−dipole mechanism, energy transfer requires that the absorption spectrum of the acceptor (here the plasmon of the metal nanoparticle) have significant overlap with the emission spectrum of the donor.[19,20,23] The plasmon band of Au ($\omega_{\text{Fröhlich}} \approx 19\,200$ cm^{-1}) can be treated as dipolar transition at approximately the same frequency as the emission from $Ru(bpy)_3^{2+}$. However, this is not the case for $Os(bpy)_3^{2+}$ on Au. Nor is the Ag plasmon in the correct spectral region to permit energy transfer from $Ru(bpy)_3^{2+}$. As observed in Figure 5, the rate constants for emission of $Ru(bpy)_3^{2+}$ adsorbed onto both Au and Ag particles are quite similar. Since Ag has a plasmon band at much higher energy ($\omega_{\text{Fröhlich}} \approx 26\,300$ cm^{-1}) than the emission of $Ru(bpy)_3^{2+}$, it is not likely that a dipole−dipole mechanism operates for $Ru(bpy)_3^{2+}$ on Ag, even if it were to operate for $Ru(bpy)_3^{2+}$ on Au nanoparticles.

There are also orientational and spin requirements for energy transfer.[20] The energy transfer probability is modulated by the angle between the transition moment of the donor and that of the acceptor. In the case of a molecule on gold, this means that the molecular transition moment must be parallel to the surface to couple into the transition dipole moment of the plasmon band. As discussed above for the observed absorption spectrum, symmetry breaking likely gives rise to a MLCT transition that is localized to a ligand perpendicular to the surface. Hence, coupling of the radiative transition to the metal could not occur as required by an energy transfer mechanism. Similar considerations apply to $Os(bpy)_3^{2+}$ where the emission spectrum is quite different, yet the time constant for deactivation on the surface of an Ag colloid is quite similar to that of $Ru(bpy)_3^{2+}$. Finally, both $Ru(bpy)_3^{2+}$ and $Os(bpy)_3^{2+}$ are excited-state triplets and energy transfer to gold would require either a spin change or a triplet state of the plasmon band on gold.

Since the spin, orientational, and spectral requirements for the dipole−dipole mechanism do not appear to be met, the mechanism for the quenching of $Ru(bpy)_3^{2+}$ and $Os(bpy)_3^{2+}$ luminescence must involve either energy transfer by the Dexter mechanism or electron transfer.[24] An electron transfer mechanism for deactivation is not only reasonable, but has precedence in a large number of metal complexes where various ligand-to-metal charge transfer states can provide a route to rapid deactivation of a molecule.[3,11,25−27] Kamat and co-workers have reported direct spectroscopic evidence for electron transfer between a gold nanoparticle and a surface-bound fluorophore induced by pulsed laser irradiation.[11,28] A classic example of this type of rapid deactivation is found in iron porphyrins where the nonradiative decay has a time constant of ca. 3 ps.[29] In the present case, the nonradiative decay times range from 400 to 1200 ps on Au and Ag nanoparticles. In other words, the observed decay times are not vastly different for $Ru(bpy)_3^{2+}$ and $Os(bpy)_3^{2+}$ complexes adsorbed onto the surfaces of Ag or Au nanoparticles. Rapid electron transfer (charge injection) from

$Ru(bpy)_3^{2+}$ or similar ruthenium complexes into TiO_2 semiconductors is well-known and has been studied to maximize the efficiency of collection of sunlight on semiconducting electrodes.[30−32] While recombination does not occur in the TiO_2 system, it likely occurs in Au and Ag nanoparticles. The sequential electron-transfer quenching mechanism is given in eq 7.

$$Ru(bpy)_3^{2+}-Au \rightarrow Ru(bpy)^*_3{}^{2+}(MLCT)-Au \rightarrow Ru(bpy)_3^{3+}-Au^- \rightarrow Ru(bpy)_3^{2+}-Au \quad (7)$$

Energy transfer by the Dexter mechanism is indistinguishable experimentally from a rapid electron transfer followed by rapid back transfer.[24] Therefore, at the present time, we can state that while electron transfer appears to be the most plausible quenching mechanism, it is not possible to rule out a Dexter energy transfer mechanism.

Conclusion

A method of determining the number of surface-adsorbed molecules has been demonstrated for both Au and Ag nanoparticles. The method provides an estimate of surface displacement reactions, since the time constant for deactivation of an adsorbed probe molecule depends on the proximity to the Au or Ag surface. For Au nanoparticles, a profound difference is observed between citrate stabilization and MO stabilization. The $Ru(bpy)_3^{2+}$ complexes displace citrate and are apparently adsorbed directly onto the nanoparticle. However, for MO-stabilized Au nanoparticles, there were three kinetic phases suggesting that some displacement occurred but that there was also a fraction of the $Ru(bpy)_3^{2+}$ complexes more loosely associated with the surface. For the MO-stabilized nanoparticle complexes, the time constant lies between that for a physisorbed complex and that for $Ru(bpy)_3^{2+}$ in solution.

Metal colloids provide a quenching mechanism that permits the quantitative measurement of the labeled adsorbates relative to the concentration of labeled species in bulk solution in a single measurement. The quenching of luminscence by nanoparticles is difficult to disentangle in a static measurement but can be quantitatively converted into surface coverage by analysis of time-resolved data. The similarity in deactivation lifetimes for all of the polypyridyl complexes adsorbed to nanoparticles suggests that electron transfer from the MLCT state to the surface followed by back electron transfer provides the dominant deactivation mechanism that competes with luminescence. The method has application to measurements of adsorptive properties in colloidal systems where varying the concentration of adsorbates may not be desirable or even possible.

Acknowledgment. S.F. gratefully acknowledges support from NSF Grant MCB-9874895.

Supporting Information Available: Steady-state emission spectra, Stern−Volmer analysis and a static quenching analysis. This material is available free of charge via the Internet at http://pubs.acs.org.

References and Notes

(1) Xie, H.; Tkachenko, A.; Glomm, W. R.; Ryan, J. A.; Brennaman, M. K.; Papanikolas, J. M.; Franzen, S.; Feldheim, D. L. *Anal. Chem.* **2003**, *75*, 5797.
(2) Thomas, K. G.; Kamat, P. V. *J. Am. Chem. Soc.* **2000**, *122*, 2655.
(3) Ipe, B. I.; Thomas, K. G.; Barazzouk, S.; Hotchandani, S.; Kamat, P. V. *J. Phys. Chem. B* **2002**, *106*, 18.
(4) Huang, T.; Murray, R. W. *Langmuir* **2002**, *18*, 7077.
(5) Forster, R. J.; Keyes, T. E. *J. Phys. Chem. B* **1998**, *102*, 10004.
(6) Fleming, C. N.; Maxwell, K. A.; DeSimone, J. M.; Meyer, T. J.; Papanikolas, J. M. *J. Am. Chem. Soc.* **2001**, *123*, 10336.
(7) Fleming, C. N.; Dupray, L. M.; Papanikolas, J. M.; Meyer, T. J. *J. Phys. Chem. A* **2002**, *106*, 2328.
(8) Shaw, G. B.; Brown, C. L.; Papanikolas, J. M. *J. Phys. Chem. A* **2002**, *106*, 1483.
(9) Franzen, S.; Folmer, J. C. W.; Glomm, W. R.; O'Neal, R. *J. Phys. Chem. A* **2002**, *106*, 6533.
(10) Thomas, K. G.; Zajicek, J.; Kamat, P. V. *Langmuir* **2002**, *18*, 3722.
(11) Kamat, P. V. *J. Phys. Chem. B* **2002**, *106*, 7729.
(12) McHale, J. L. *Molecular Spectroscopy*, 1st ed.; Prentice Hall: Upper Saddle River, NJ, 1999.
(13) Oh, D. H.; Boxer, S. G. *J. Am. Chem. Soc.* **1989**, *111*, 1130.
(14) Houten, V.; Watts, R. J. *J. Am. Chem. Soc.* **1976**, *98*, 8.
(15) Sudeep, P. K.; Ipe, B. I.; Thomas, K. G.; George, M. V.; Barazzouk, S.; Hotchandani, S.; Kamat, P. V. *Nano Lett.* **2002**, *2*, 29.
(16) Wang, G. L.; Zhang, J.; Murray, R. W. *Anal. Chem.* **2002**, *74*, 4320.
(17) Javier, A.; Yun, C. S.; Sorena, J.; Strouse, G. F. *J. Phys. Chem. B* **2003**, *107*, 435.
(18) Lakowicz, J. R.; Shen, Y.; D'Auria, S.; Malicka, J.; Fang, J.; Gryczynski, Z.; Gryczynski, I. *Anal. Biochem.* **2002**, *301*, 261.
(19) Sirota, M.; Minkin, E.; Lifshitz, E.; Hensel, V.; Lahav, M. *J. Phys. Chem. B* **2001**, *105*, 6792.
(20) Dulkeith, E.; Morteani, A. C.; Niedereichholz, T.; Klar, T. A.; Feldmann, J.; Levi, S. A.; van Veggel, F.; Reinhoudt, D. N.; Moller, M.; Gittins, D. I. *Phys. Rev. Lett.* **2002**, *89*, art. no. 203002.
(21) Perez-Luna, V. H.; Yang, S. P.; Rabinovich, E. M.; Buranda, T.; Sklar, L. A.; Hampton, P. D.; Lopez, G. P. *Biosens. Bioelectron.* **2002**, *17*, 71.
(22) Maxwell, D. J.; Taylor, J. R.; Nie, S. M. *J. Am. Chem. Soc.* **2002**, *124*, 9606.
(23) Forster, T. *Discuss. Faraday Soc.* **1959**, *27*, 7.
(24) Altarell, M.; Dexter, D. L. *Phys. Rev. B* **1973**, *7*, 5335.
(25) Nikoobakht, B.; Burda, C.; Braun, M.; Hun, M.; El-Sayed, M. A. *Photochem. Photobiol.* **2002**, *75*, 591.
(26) Enger, O.; Nuesch, F.; Fibbioli, M.; Echegoyen, L.; Pretsch, E.; Diederich, F. *J. Mater. Chem.* **2000**, *10*, 2231.
(27) Kamat, P. V.; Shanghavi, B. *J. Phys. Chem. B* **1997**, *101*, 7675.
(28) Kamat, P. V.; Flumiani, M.; Dawson, A. *Colloids Surf., A* **2002**, *202*, 269.
(29) Franzen, S.; Kiger, L.; Poyart, C.; Martin, J. L. *Biophys. J.* **2001**, *80*, 2372.
(30) Kuciauskas, D.; Monat, J. E.; Villahermosa, R.; Gray, H. B.; Lewis, N. S.; McCusker, J. K. *J. Phys. Chem. B* **2002**, *106*, 9347.
(31) Yang, M.; Thompson, D. W.; Meyer, G. J. *Inorg. Chem.* **2002**, *41*, 1254.
(32) Kalyanasundaram, K.; Gratzel, M. *Coord. Chem. Rev.* **1998**, *177*, 347.